Proceedings of
The Second National Congress on Fluids Engineering
August 22-24, 2002, Muju, Korea

Effects of Non-Uniform Inflow on Aerodynamic Behaviour of Horizontal Axis Wind Turbine

Koji KIKUYAMA, Yutaka HASEGAWA and Kai KARIKOMI
Dept. of Mechanical Eng., Nagoya University
Furo-cho, Chikusa-ku, Nagoya 464-8603, Japan
phone: +81-52-789-2710, fax: +81-52-789-5123, e-mail: kikuyama@mech.nagoya-u.ac.jp

ABSTRACT: Non-uniform and unsteady inflow into a Horizontal Axis Wind Turbine (HAWT) brings about an asymmetric flow field on the rotor plane and an unsteady aerodynamic load on the blades. In the present paper effects of yawed inflow and wind shear are analyzed by an inviscid aerodynamic model based on the asymptotic acceleration potential method. In the analysis the rotor blades are represented by spanwise and chordwise pressure distribution composed of analytical first-order asymptotic solutions for the Laplace equation. As the actual wind field experienced by a HAWT is turbulent, the effects of the turbulence are also examined using the Veers' model.

Keywords: Horizontal Axis Wind Turbine, Numerical Method, Aerodynamic Load, Yawed Inflow, Wind Shear, Turbulence

1. Introduction

Horizontal Axis Wind Turbines (HAWTs) installed in the open air are subject to the non-uniform in space and unsteady in time wind conditions due to the yawed inflow, wind shear and time dependant fluctuating flow. With increase in the diameter and output of wind turbines, clarifying the effects of these inflow conditions on the load, performance and fatigue damage has become more important for the design of the rotor blades and the control systems.

In a yawed condition the structure of wake vortices emitted from the rotor blades inclines to the rotating axis, resulting in an asymmetric induced velocity distribution on the rotor plane. Velocities relative to the rotating blade periodically change with its azimuthal position due to the inclined undisturbed wind velocity as well as the asymmetric induced velocity distribution. Thus the strength of the wake vorticity also changes periodically, which generates an additional change in the induced velocity in the rotor plane. On the other hand, the wind turbine working near the ground is subject to the vertical wind shear, resulting in a cyclic change of the load on each blade.

In addition to the above effects, turbulence brings about complicated aerodynamic loads, sometimes resulting in unexpected fatigue damage on the rotor. Thus, clarification of the turbulent wind effects on the loads and performance of HAWT rotors has become an up-to-date topic for the design of the rotor blades.

The present paper shows the calculating results of the aerodynamic loads on the rotor blades of HAWT. The calculation model used is based on an asymptotic acceleration potential method under the assumption of incompressible, inviscid and irrotational flow around the wind turbine rotor. The Laplace equation with respect to the pressure perturbations is introduced. With the use of the analytical first-order asymptotic solutions of the equation, the rotor blades are represented by spanwise and chordwise pressure distributions.

2. Acceleration Potential Method

Basic equations

An inviscid aerodynamic model based on the asymptotic acceleration potential method is adopted for the calculation of aerodynamic loads on the blades[1][2].

Assuming incompressible and inviscid flow around a wind turbine rotor, the governing equations are the Euler equation and the continuity equation. The Euler equation can be linearized by assuming that the induced velocities are small enough against the undisturbed velocity. Taking divergence of the linearized Euler equation and with the assumption of irrotational flow, the Laplace equation of the pressure perturbation is derived, using the Cartesian coordinate system in Fig.1, as follows

$$\nabla^2 p = \frac{\partial^2 p}{\partial x^2} + \frac{\partial^2 p}{\partial y^2} + \frac{\partial^2 p}{\partial z^2} = 0 \qquad (1)$$

The pressure perturbation acts on air particles as acceleration potential function.

The rotor blades can be represented by spanwise and chordwise pressure distributions, which are composed of analytical first-order asymptotic solutions of the Laplace equation.

Integration of the acceleration experienced by the

particles of air, which travel from far upstream to the rotor blade, determines the velocities including the induced velocities in the rotor plane. With these velocities, the aerodynamic loads can be calculated for the moment at which the air particles arrive at the rotor plane.

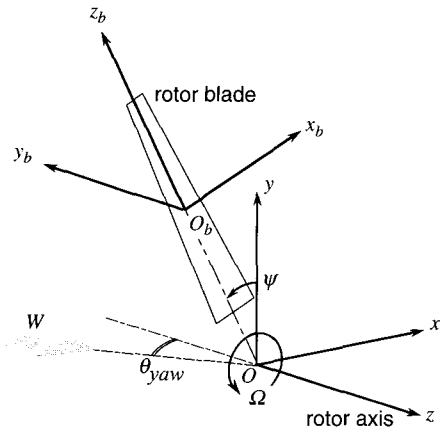

Figure 1: Coordinate system and yawed inflow

Approximate solution method

The Laplace equation of the pressure has been solved by adopting approximate solution techniques listed below:
(i) asymptotic expansion method of the first-order for the pressure field around the rotor
(ii) spanwise lift distributions expressed by finite series of associate Legendre functions.

At considerable distance from the rotor blade (lifting surface), the experienced accelerations are equivalent to those caused by a lifting line, on which the load is concentrated. Therefore in the far field, the blade can be modeled with a pressure dipole line that gives the three-dimensional pressure distribution around the rotor blade, i.e., p_{far} .

Close to the blade, the experienced accelerations are dominated by the chordwise load distributions. Thus the accelerations can be modeled with two-dimensional pressure distributions p_{near} around the blade section in the near field.

These two asymptotic approximations are combined with the use of the third term (a common field term p_{common}), which cancels the far field term near the lifting surface, as well as the near field term far away from the surface.

The sum of the three terms of the pressure perturbation gives an expression that is valid in the whole field.

$$p_{composite} = p_{near} + p_{far} - p_{common} \qquad (2)$$

In the application of asymptotes, only the first order term is considered for each field and the solutions are adopted in the present code.

Using a local coordinate (x_b , y_b , z_b) system shown in Fig. 1, the boundary conditions for the problem are

$$p = 0 \quad for\ x_b^2 + y_b^2 + z_b^2 \to \infty \qquad (3)$$

$$\frac{\partial p}{\partial y_b} = 0 \quad on\ rotor\ blade \qquad (4)$$

$$\frac{w}{\Omega r} = \theta_p \quad on\ rotor\ blade \qquad (5)$$

where θ_p denotes a spanwise distribution of the blade pitching angle.

The first condition is obvious from the definition of the function p as the pressure perturbation. The second means that the flow on a flat plate airfoil located in the x_b - z_b plane does not experience the acceleration normal to the airfoil. The third one, where w is the axial velocity including the induced velocity and r is the radial position, is the kinematic condition on the rotor blade, i.e., Kutta's condition.

Integration method

Application of the kinematic boundary condition (the Kutta's condition) is tackled with numerical methods. For the kinematic boundary condition, the velocity can be calculated by integrating the acceleration of the air particle, which goes to each collocation point. The collocation points where the kinematic boundary condition must be satisfied are located on half chord lines of each blade at different spanwise distance.

Suppose the pressure field is known at every instant, the accelerations in the field can be determined, thus the paths of the air particles and their velocities in the rotor plane can also be found. The paths are, however, unknown a priori, since they are determined by a pressure field that still includes unknown coefficients. In order to determine the coefficients an iterative calculation for the pressure and the path is repeated at each time step. This iterative process brings about a delinearized path, which corresponds to the wake relaxation in the vortex representation. In this sense, the present calculation method includes the free wake model.

3. Calculation condition

The calculation has been performed for the geometry of the Danish Tjaereborg wind turbine, which is three bladed rotor with radius R of 30.56 [m]. Its rotational speed in operation Ω is 22 [rpm] and the optimum tip speed ratio is $\lambda = \Omega R/W = 8$, where W denotes the undisturbed wind speed far upstream from the rotor.

Yawed inflow

The undisturbed velocity is assumed as shown in Fig.1. Let the rotor axis lie on the z-axis and rotor plane in the x-y plane, the undisturbed wind direction is assumed to have a misalignment angle of θ_{yaw} to the z-axis in the z-x plane and

the velocity components are given as

$$V = \left(W \sin\theta_{yaw}, 0, W \cos\theta_{yaw}\right) \tag{6}$$

Wind shear

The wind speed far upstream at the height of $(H + y)$ above the ground is given by the following equation.

$$W(y) = W_{hub} \frac{\ln[(y+H)/z_0]}{\ln(H/z_0)} \tag{7}$$

where H denotes the hub height of the rotor, taken to be 60m in the calculation, and W_{hub} represents the undisturbed wind speed at the hub height. The value of z_0 is the roughness length of the ground surface. In this paper, it is assumed that z_0 = 0.025, 0.3 and 1.0 correspond to the grassland, farm and forest, respectively. The velocity profiles for these roughness values are shown in Fig. 2.

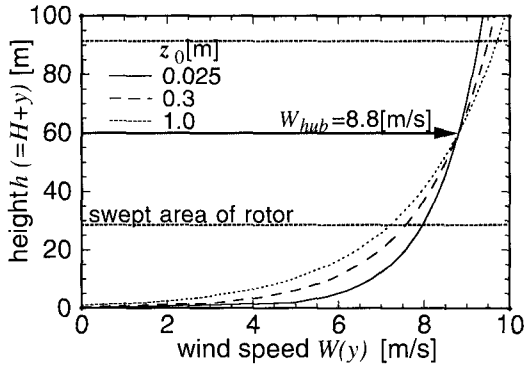

Figure 2: Wind shear profile

Turbulent wind field

The turbulent wind field around the rotor is schematically shown in Fig.3., and can be separated into two parts, i.e., a deterministic part and a stochastic part. The former is the wind shear profile and the latter the turbulence components. For the wind shear, the power law profile is adopted with wind shear exponent of 0.2. On the other hand, the turbulence is simulated by the Veers' model[3]. For the turbulence component, the PSD and coherence function are given by the von Karman spectrum and the exponential coherency model respectively. The power spectral density (PSD) of longitudinal wind speed fluctuations at a point i can be written as

$$S_{ii}(f) = \frac{4\sigma^2 L/W_{hub}}{\left[1+71(fL/W_{hub})^2\right]^{5/6}} \tag{8}$$

where σ is the standard deviation of the longitudinal wind speed and W_{hub} is the 10-minute averaged wind speed at hub height H. The isotropic integral scale parameter L is defined by using the turbulence scale parameter Λ as follows

$$L = 3.5\Lambda \quad where \quad \Lambda = \min\ (0.7H,\ 21) \tag{9}$$

The exponential coherence function for the point i and j is described as

$$Coh_{ij}(d,f) = \exp\left[-8.8\left((fr/W_{hub})^2 + (0.12r/L)^2\right)^{1/2}\right] \tag{10}$$

where d is the distance between two points in the rotor plane, and this model assumes that the coherence is not dependent on the height or direction of the points.

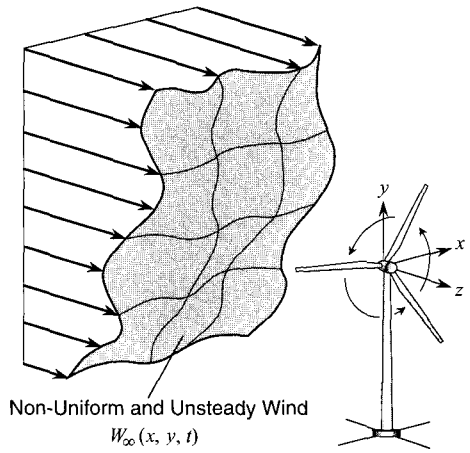

Figure 3: Turbulent wind model

4. Calculation results and discussions

Yawed inflow effects

Figure 4 shows the calculation results for the axial induced velocity wind on the rotor blade when the inflow direction is inclined to the rotating axis as much as θ_{yaw} = 30 [deg], and the tip speed ratio λ = 8 . Azimuth angle of the blade position ψ is taken to be measured unti-clockwise from the vertical axis (y-axis) as shown in Fig. 1.

At the yaw misalignment θ_{yaw} = 30 [deg], the normalized induced velocity w_{ind}/W at r/R = 0.88 fluctuates largely with azimuth position and takes its minimum at ψ = 90 [deg], where the blade is far apart from the inclined wake. The induced velocity at r/R = 0.34, however, decreases in the vicinity of ψ = 270 [deg] due to the effect of the trailing vortex emitted from the foregoing blade's root.

In Fig. 5 the calculated yaw moment is compared with the experimental results obtained by Friis et. al [5] for Tjaereborg turbine at tip speed ratio λ of 8.8. Though the experimental data has some offset at θ_{yaw} = 0 [deg] and scatter for all the values of θ_{yaw} , the calculation result shows good agreement with the measurement in the range of the yaw angle between approximately -30 and +30 [deg].

The dynamic yaw calculations have been carried out for stepwise change of the yawed inflow angle within the time of Δt = 0.0758[s], which corresponds to the period of 1/36 rotation of the rotor.

The calculated results for the power coefficients are plotted as a function of time in Fig 6 in which dimensionless time t/T_0 for abscissa is equal to the number of rotor revolution. The rotor shaft torque of the three-bladed rotor is seen to fluctuate with the period of 1/3 rotation. After the step in the yaw angle the torque shows a transient behavior and takes a few revolutions before it attains a quasi-stationary state of the wake vortex structure for the constant yaw condition.

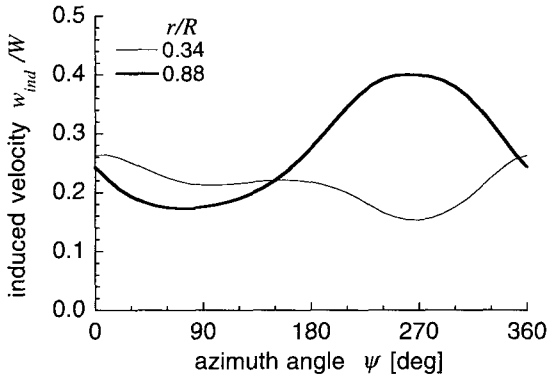

Figure 4: Induced velocity fluctuation

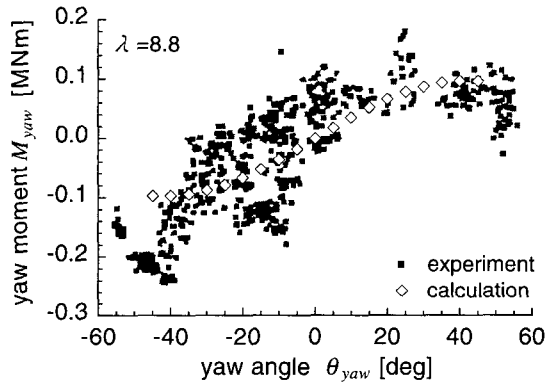

Figure 5: Comparison of calculated yaw moment with experimental results [5]

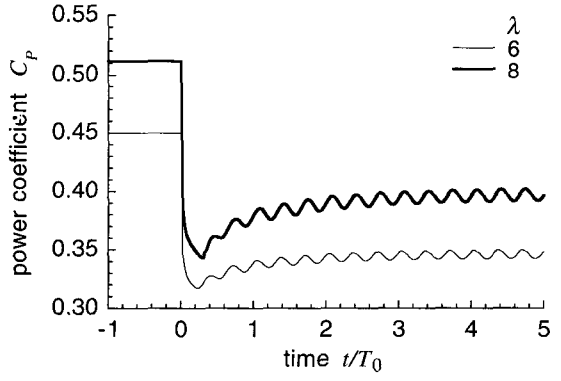

Figure 6: Power coefficient response against stepwise change of yaw angle

Wind shear effects

Figure 7 and 8 show the contours of the induced velocity and local lift coefficient on rotor. The induced velocity exhibits asymmetric distribution in the vertical direction and is increased in the lower part of the plane because the spatial interval of the trailing vortex is shortened due to the decreased main velocity in the lower part of the plane.

The effect of the wind shear profile and the asymmetric distribution of induced velocity lead to the inhomogeneous distribution of the lift coefficient. In contradiction to the induced velocity distribution, the lift coefficient takes the larger values in the upper part of the plane than the lower part, resulting in a periodic change in the flapwise moment on the blade M_{flp}.

Figure 9 shows the change in M_{flp} for different tip speed ratios during a rotation for different wind shear profile. With the increase in the roughness, that is, the velocity gradient near the ground, the fluctuation of the flapwise moment is increased.

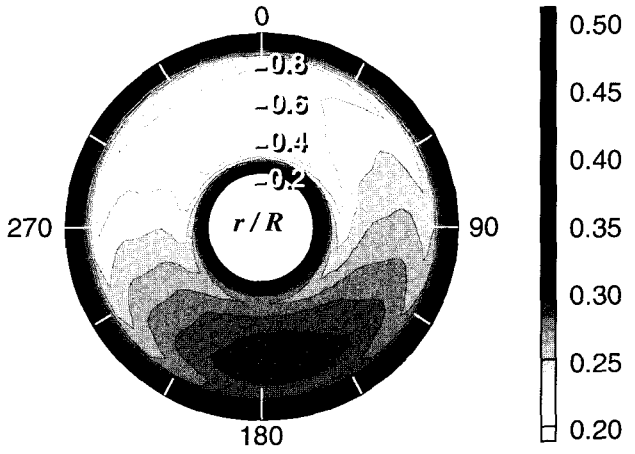

Figure 7: Induced velocity distribution on rotor plane

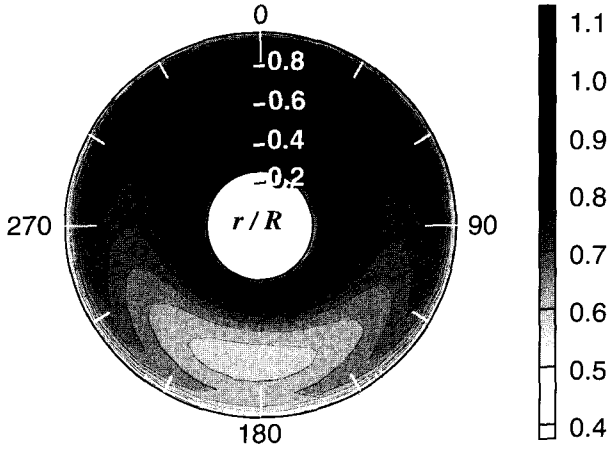

Figure 8: Lift coefficient distribution on rotor plane

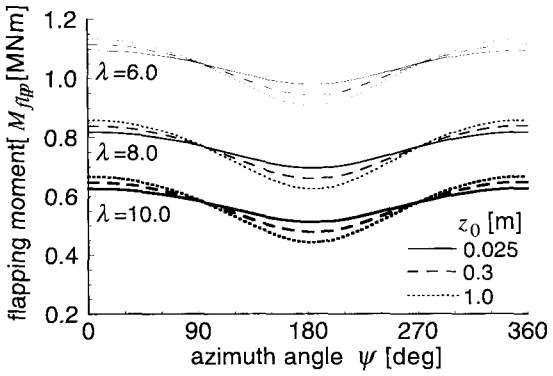

Figure 9: Flapwise moment fluctuation for various roughness lengths and wind speeds at hub height

Turbulent inflow effects

Figure 11 shows examples of the simulated wind time series at 4 points located in the rotor plane in Fig.10 under the condition that the standard deviation of wind speed σ, the mean wind speed at hub height W_{hub}, and the turbulence length scale L are 8.8 [m/s], 1.0 [m/s] and 73.5 [m], respectively.

The difference in the time averaged wind speeds between the upper 2 points (a1 and a2) and the lower 2 points (b1 and b2) is due to the wind shear. It can be found that the correlation between the two wind time series at upper (or lower) two points is good, however, poor between those at upper and lower points.

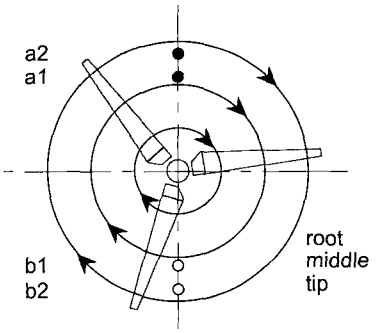

Figure 10: Sampling points for Fig. 11,12 and 13

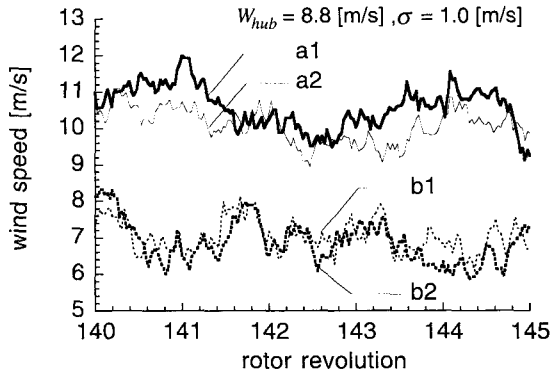

Figure 11: Simulated wind time series

Power spectra of the turbulent inflow are presented in Fig.12 for the different points in the rotor plane together with the theoretical von Karman spectrum for comparison. It can be seen that the statistical properties of the simulated wind are consistent with the given spectrum.

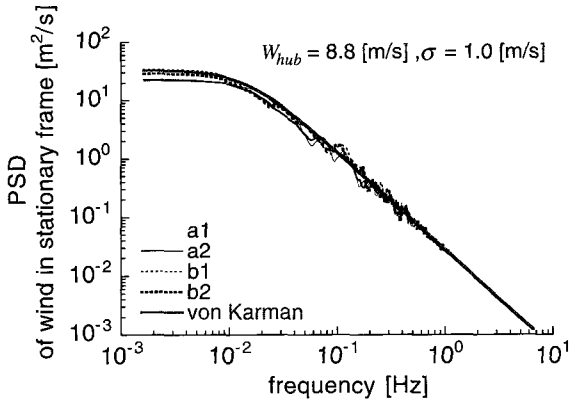

Figure 12: Power spectrum of simulated wind and von Karman spectrum

The stochastic properties of the wind that is actually experienced by the rotating blades, however, are considerably different from those obtained in the stationary frame in Fig.1. The spectra of undisturbed axial velocities experienced at three different spanwise positions on the blade, that is, near the root (34% spanwise position) , middle (58%) and tip (88%) of the blade (see Fig.10), are plotted in Fig.13. The rotational sampling of the turbulent wind field that has a spatial non-uniform structure generates spikes of the spectrum at the multiples of the rotation frequency (=0.37 [Hz]). This non-uniform spatial structure, which depends not only on the wind shear profile but also on the turbulence component, causes the fluctuation of aerodynamic loads on blades.

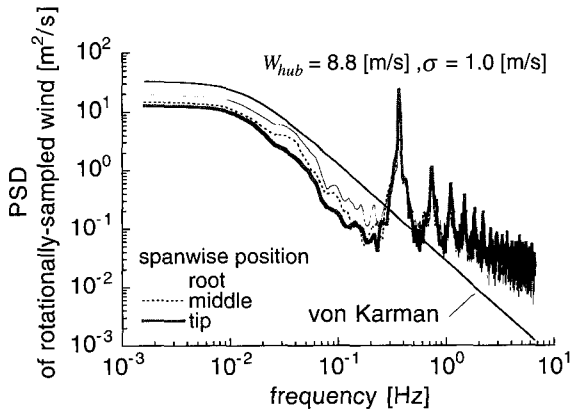

Figure 13: Power spectrum of undisturbed wind experienced by blade

The calculated time series of flapwise moment at the blade root is plotted in Fig.14 under the condition of W_{hub} =

8.8 [m/s] and L = 73.5 [m] with various standard deviations σ. The fluctuation of the moment for σ = 0.0 , which corresponds to the vertically sheared inflow without any turbulence, depicts approximately sinusoidal wave. Addition of the turbulence to the shear profile causes the complex fluctuation, and the larger turbulence brings about the larger amplitude of the fluctuation.

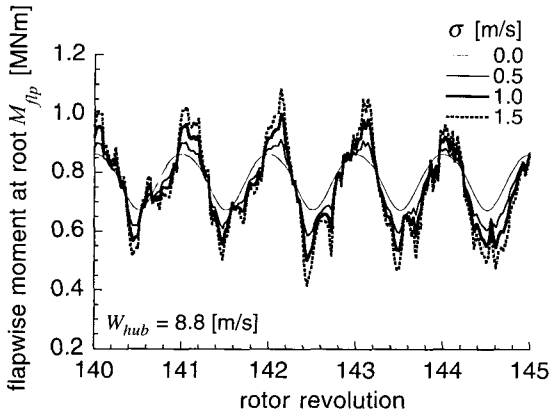

Figure 14: Time series of flapwise moment

Figure 15 shows the power spectral densities of the flapwise moments. Characteristic spikes in the spectrum are similar to those of the PSD of rotationally-sampled wind in Fig.13. The dominant 1P (one cycle per rotor revolution) component of the load fluctuation is due to the wind shear profile. Though the spectrum for different degree of turbulence is seen to be similar to each other, the increase in σ causes larger fluctuation, leading to the increment of fatigue loads.

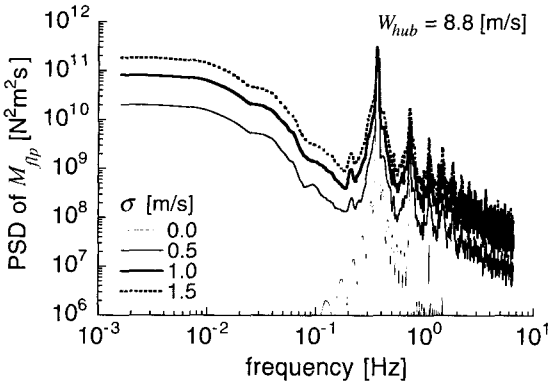

Figure 15: Power spectrum of flapwise moment in Fig.14

5. Concluding remarks

Effects of the non-uniform and unsteady inflow conditions on the induced velocity and the aerodynamic loads on a Horizontal Axis Wind Turbine (HAWT) has been analyzed by the asymptotic acceleration potential method, assuming an incompressible and inviscid flow around the turbine. The major results obtained are summarized as follows.

- The yawed inflow causes an asymmetric flow field on the rotor plane and unsteady aerodynamic loads on the blades. The flapwise moment exerted on the blade, which causes the blade to bend downstream, is increased with the yaw angle of inflow. The yaw moment, which is deduced by taking the vector summation of the flapwise moments on all the blade, was found to agree well with the experimental data.
- The wind shear brings about an asymmetric distribution of the induced velocity and lift coefficient. The induced velocity is increased in the lower part of the rotor plane and decreased in the upper part due to the deformed configuration of the spiral trailing vortex downstream of the plane.
- The turbulence of the inflow into the turbine rotor gives rise to the complicated fluctuation of the aerodynamic loads, and the increase of the turbulence augments the load fluctuation. The turbulence effects must be considered in the structural design process of rotor blades.

References

[1] van Holten, Th. ,The computation of aerodynamic loads on helicopter blades in forward flight using the method of the acceleration potential, Report VTH-189, Delft Univ. Tech.,Delft, The Netherlands, 1975.

[2] van Bussel, G. J. W., The use of asymptotic acceleration potential methods for horizontal axis windturbine rotor aerodynamics, Proc. EWEC'91, Amsterdam, pp. 18-23, 1991.

[3] Veers, P. S., Three-Dimensional Wind Simulation, SAND-88-0152, Sandia National Laboratories, Albuquerque, NM, 1988.

[4] IEC 61400-1, 2nd ed., Wind Turbine Generator Systems - Part 1: Safety Requirements, 1999.

[5] P. Friis, M. Knudsen, K. S. Hansen, Proc. EWEC'93 Conf. Lubeck-Travemunde (1993) 243.